ACADÉMIE
DES SCIENCES
INSTITUT DE FRANCE

Comptes Rendus
Mécanique

Pietro Cornetti, Vladislav Mantič and Zohar Yosibash

3D finite fracture mechanics under mode I loading: the flat elliptical crack

Volume 353 (2025), p. 725-745

Online since: 16 June 2025

https://doi.org/10.5802/crmeca.302

The Comptes Rendus. Mécanique *are a member of the Mersenne Center for open scientific publishing*
www.centre-mersenne.org — e-ISSN : 1873-7234

ACADÉMIE DES SCIENCES
INSTITUT DE FRANCE

Comptes Rendus. Mécanique
2025, Vol. 353, p. 725-745
https://doi.org/10.5802/crmeca.302

Research article / *Article de recherche*

3D finite fracture mechanics under mode I loading: the flat elliptical crack

Mécanique de la rupture finie en 3D sous chargement en mode I : la fissure elliptique plane

Pietro Cornetti[*,a], **Vladislav Mantič**[b] **and Zohar Yosibash**[c]

[a] Department of Structural, Geotechnical and Building Engineering, Politecnico di Torino, Corso Duca degli Abruzzi 24, 10129 Torino, Italy

[b] Grupo de Elasticidad y Resistencia de Materiales, Escuela Técnica Superior de Ingeniería, Universidad de Sevilla, Camino de los Descubrimientos s/n, Sevilla, 41092, Spain

[c] Computational Mechanics and Experimental Biomechanics Lab, School of Mechanical Engineering, Iby and Aladar Fleischman Faculty of Engineering, Tel Aviv University, Ramat Aviv 69978, Israel

E-mail: pietro.cornetti@polito.it (P. Cornetti)

Abstract. The determination of the remote stress causing crack propagation in an infinite 3D domain with an embedded flat elliptical crack is here revisited in the framework of the Coupled Criterion of Finite Fracture Mechanics. We started reviewing Linear Elastic Fracture Mechanics approaches, which differ by accounting for different infinitesimal crack growths. Then, we provide the solution based on Finite Fracture Mechanics: if the elliptical flaw is sufficiently small, the crack grows along iso-stress lines. For larger sizes, other crack growths may take place. Thus, the present investigation shows that assuming an iso-stress crack front may effectively provide the exact Finite Fracture Mechanics solution, particularly for small defects; on the other hand, it can be wrong for larger size, providing moreover un-conservative predictions. However, for the geometry at hand, it yields failure stress estimates differing from the actual one by a few percents. Thus, the iso-stress assumption, conjectured by Leguillon [D. Leguillon, "An attempt to extend the 2D coupled criterion for crack nucleation in brittle materials to the 3D case", *Theor. Appl. Fract. Mech.* **74** (2014), pp. 7–17]—implying strong simplifications in the numerical implementation of the coupled criterion in 3D problems—seems to be largely justified by the present results. Moreover, regardless of the initial crack size, the finite growth predicted by the model results in a new elliptical crack shape closer to the circular one, meaning the eccentricity consistently decreases as the crack propagates.

Résumé. La détermination de la contrainte à distance provoquant la propagation d'une fissure dans un domaine 3D infini contenant une fissure elliptique plane est ici revisitée dans le cadre du Critère Couplé de la Mécanique de la Rupture Finie. Nous commençons par passer en revue les approches de la Mécanique Linéaire de la Rupture, qui diffèrent selon la prise en compte de différentes croissances infinitésimales de la fissure. Ensuite, nous présentons la solution basée sur la Mécanique de la Rupture Finie : si le défaut elliptique est suffisamment petit, la fissure croît le long de lignes iso-contraintes. Pour des tailles plus grandes, d'autres modes de croissance de fissure peuvent se produire. Ainsi, cette étude montre que supposer un front de fissure iso-contraintes peut effectivement fournir la solution exacte en Mécanique de la Rupture Finie, en particulier pour les petits défauts ; en revanche, cela peut être erroné pour des défauts de plus grande taille, entraînant de surcroît des prédictions non conservatrices. Toutefois, pour la géométrie considérée,

* Corresponding author

cela donne des estimations de contrainte de rupture ne différant que de quelques pourcents de la valeur réelle. Ainsi, l'hypothèse d'iso-contraintes, avancée par Leguillon [D. Leguillon, "An attempt to extend the 2D coupled criterion for crack nucleation in brittle materials to the 3D case", *Theor. Appl. Fract. Mech.* **74** (2014), pp. 7-17], impliquant des simplifications importantes dans l'implémentation numérique du critère couplé dans des problèmes 3D, semble largement justifiée par les résultats présents. En outre, quelle que soit la taille initiale de la fissure, la croissance finie prédite par le modèle aboutit à une nouvelle forme elliptique de la fissure, plus proche d'un cercle, ce qui signifie que l'excentricité diminue systématiquement au fur et à mesure de la propagation de la fissure.

Keywords. Coupled criterion, Finite fracture mechanics, 3D linear elastic fracture mechanics, Elliptical cracks, Quasi-brittle materials.

Mots-clés. Critère couplé, Mécanique de la rupture finie, Mécanique de la fracture élastique linéaire en 3D, Fissures elliptiques, Matériaux quasi-fragile.

Funding. NEWFRAC Project (Marie Sklodowska-Curie grant agreement No. 861061), Pazy Research Foundation, Spanish Ministry of Science and Innovation, European Regional Development Fund (PID2021-123325OB-I00).

Manuscript received 6 February 2025, revised 17 May 2025, accepted 19 May 2025.

1. Introduction

The Coupled Criterion of Finite Fracture Mechanics (CCFFM), introduced for the first time by Leguillon [1] in 2002, has proven to be an effective, yet simple, fracture criterion for obtaining the failure load in a variety of structural problems, spanning from size effect (e.g. [2]) to stress concentration/intensification (e.g. [3–5]) in homogeneous materials, from composite materials (e.g. [6–8]) to bonded joints (e.g. [9]), from static loadings to dynamic (e.g. [10,11]) and fatigue (e.g. [12,13]) loadings. With respect to Linear Elastic Fracture Mechanics (LEFM), a major advantage is its applicability to any geometry, cracked or plain (i.e. not only cracked). With respect to more sophisticated models like the Cohesive Crack Model (CCM) or the Phase Field (PF) model for fracture, the numerical implementation of the CCFFM is usually much easier, often allowing for an analytical or semi-analytical solution for the problem at hand. Moreover, the CCFFM has proven to be often in agreement with CCM and PF models: for a comparison between CCFFM and CCM the reader is referred to [14–19]; and for a comparison between CCFFM and PF to [20–24].

Most of the CCFFM applications address two-dimensional problems, where cracks/V-notch tips are straight lines through-the-thickness. However, recently, attention has also been focussed to 3D problems, starting from Leguillon's pioneering work [25]. The application of the CCFFM to 3D problems is challenging because the finite crack advance, differently from the 2D case, can be of any shape [26]. To overcome this difficulty, researchers often assumed a finite crack growth occurring along an iso-stress line, see e.g. [27–29]. One of our main purposes is investigating this assumption for a model problem allowing an analytical derivation in the framework of the CCFFM: a flat elliptical flaw in an infinite linear elastic medium subjected to a remote tensile stress orthogonal to the crack plane.

The linear elastic stress-strain solution for an elliptical flaw under remote tensile stress dates back to Green and Sneddon [30], following (and including) the one for a penny-shaped crack provided by Sneddon [31]. Later, Irwin [32] provided the Stress Intensity Factor (SIF) values along the elliptical crack front. More recent contributions related to the stress field in the vicinity of the crack front can be found in [33,34]. For what concerns crack propagation, Lazarus [35], among different flaw shapes, considered the elliptical one and analysed the crack growth for a brittle fracture (assuming propagation where the SIF reaches the fracture toughness and regularising the crack front) and fatigue (using Paris' equation). More numerical/practical contributions along with experimental data validation (under cycling loading) about crack propagation from

flat elliptical cracks can be found, e.g., in [36–38]. Finally, we refer to a recent numerical investigation where the CCFFM criterion has been exploited to deal with free edge delamination in angle-ply laminates, assuming a semi-elliptical crack shape, under static [39], fatigue [40] and thermal [41] loadings. These papers provide details on the numerical implementation of the Coupled Criterion for geometries similar to the one addressed herein.

The paper is organised as follows. In Section 2 we focus on LEFM, deriving the general expression of the mode I failure stress in the presence of a flaw of any shape under the assumption of an infinitesimal iso-stress crack growth. Then, we specify the failure stress for the flat elliptical crack, providing its closed form estimate by means of SIFs. Thereafter, we show the same result can be achieved by evaluating the Strain Energy Release Rate (SERR). Following this latter procedure, we also consider the infinitesimal elliptical crack growth along the minor axis alone, showing it provides failure stress estimates lower than the iso-stress one.

In Section 3 we derive the failure stress provided by the CCFFM for the flat elliptical crack. We assume the finite crack propagation to be characterised by an elliptical crack front of any shape/size. Thus, the new crack front is characterised by two parameters (the increments of the semi-axes); CCFFM implies solving a minimisation problem upon the variation of these two parameters. It will be shown that, based on the crack shape and size, two different scenarios (i.e. iso-stress and minor-axis crack propagations) can occur and the corresponding fracture stress is finally provided. The results are commented and in Section 4 some conclusions are drawn.

2. LEFM approach

We first provide the failure stress according to LEFM for a flat crack with an arbitrary shape subject to a mode I loading, then specify it for the elliptical crack. Two procedures, based on SIF or SERR, are outlined and exploited.

2.1. *Planar crack of arbitrary shape: iso-stress crack growth*

Let us consider a planar crack of arbitrary shape in an infinite body, made by a homogeneous isotropic linear elastic brittle material. Let the plane of the crack be (x, y). The remote loading is a uniform tensile stress σ in the z direction as in Figure 1. Under this assumption the crack is in pure mode I condition (or—the same—in opening mode, since, because of isotropy, the displacement field is symmetrical to the crack plane).

Except for the penny-shaped crack, the SIF varies along the contour C of the crack, i.e. $K_I = K_I(s)$, s being the curvilinear abscissa along the contour C (Figure 1b). Denoting by $K_{I,\min}$ and the by $K_{I,\max}$ the minimum and maximum value of the SIF respectively, we can write:

$$K_{I,\min} \le K_I(s) \le K_{I,\max}. \tag{1}$$

Assume $K_I = K_I(s)$ is available in an analytic or numerical form, and the fracture toughness K_{Ic} of the material is known. One is interested in σ_{f}, the remote stress causing crack growth, i.e. failure, according to LEFM. Because of mode I, the crack expands in its plane (x, y). However, if one wishes to consider the Griffith's SERR, there are an infinite possible shapes of infinitesimal crack growth, unlike in 2D domains where only a collinear crack growth is possible along an infinitesimal length da (a being the crack length).

A reasonable starting point is assuming (yet, an assumption) an infinitesimal crack growth defined by an iso-stress line. Since the asymptotic stress field in the direction normal to the crack contour (r is the coordinate along the normal $\hat{n}$ starting from the crack contour C, see Figure 1b) is:

$$\sigma_z \cong \frac{K_I}{\sqrt{2\pi r}} \tag{2}$$

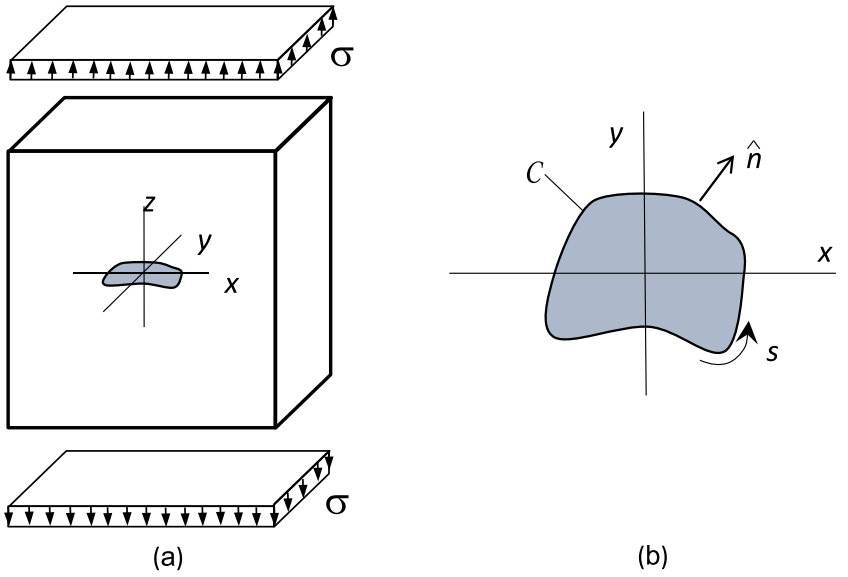

Figure 1. A planar crack of arbitrary shape in an infinite 3D domain under uniform tensile stress normal to the crack plane (a). Crack geometry (b).

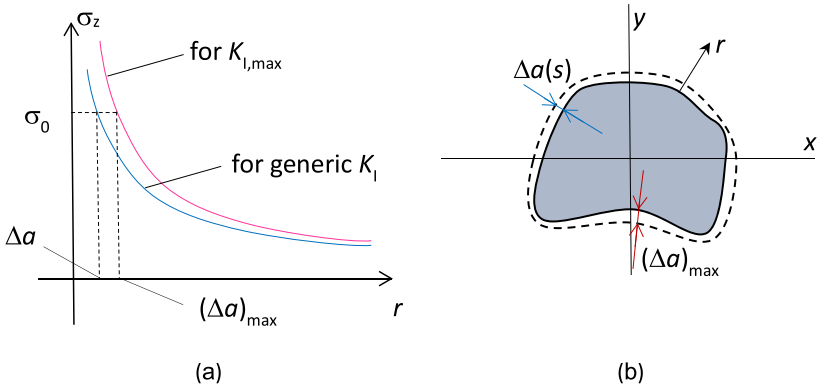

Figure 2. Asymptotic stress field ahead the crack front (a) and iso-stress crack growth (b).

The same stress level (e.g. σ_0) is achieved at different distances from the contour C, larger where K_I is larger, smaller where K_I is smaller (see Figure 2a). Where K_I is maximum, the stress σ_0 is achieved at a distance $(\Delta a)_{\max}$:

$$(\Delta a)_{\max} \cong \frac{K_{I,\max}^2}{2\pi\sigma_0^2} \tag{3}$$

while in a generic point we have:

$$(\Delta a) \cong \frac{K_I^2}{2\pi\sigma_0^2} \tag{4}$$

Dividing Equation (3) by (4), one obtains:

$$\frac{\Delta a}{(\Delta a)_{\max}} \cong \left(\frac{K_I}{K_{I,\max}}\right)^2 = \frac{G}{G_{\max}} \tag{5}$$

where the last expression is a consequence of Irwin's relationship $G = K_I^2/E'$, G being the SERR and E' the Young modulus of the material under plane strain conditions. As Δa tends to zero, Equation (5) defines the shape of the infinitesimal iso-stress crack growth (see Figure 2b).

Expressing the Griffith infinitesimal energy balance according to LEFM (G_c being the material fracture energy) by an integral along the curve C, one obtains:

$$\oint_C G(s)\Delta a\,\mathrm{d}s = \oint_C G_c \Delta a\,\mathrm{d}s \tag{6}$$

Dividing both sides of Equation (6) by $(\Delta a)_{\max}$ and substituting Equation (5) into Equation (6), one obtains the condition for crack growth:

$$G_{\text{iso}} = \frac{\oint_C G^2(s)\,\mathrm{d}s}{\oint_C G(s)\,\mathrm{d}s} = G_c \tag{7}$$

The ratio between the integrals is somehow an equivalent-2D SERR, since crack growth occurs whenever this value reaches the material fracture energy G_c, like in 2D problems. We named it G_{iso} since it is the equivalent-2D SERR under the assumption of iso-stress crack growth. Note that, from a mathematical point of view, G_{iso} is the contra-harmonic mean (sum of the squared values divided by sum of values, see Appendix A) of the SERR values evaluated along the crack contour. Among different averages (i.e. harmonic, geometric, arithmetic, quadratic, etc.) the contra-harmonic mean is the highest one, thus affected by large values and close to the maximum value of the variable. By Irwin's relationship we can get also the equivalent-2D SIF $K_{I,\text{iso}}$, which provides the failure stress when it equals the material fracture toughness K_{Ic}:

$$K_{I,\text{iso}} = \sqrt{\frac{\oint_C K_I^4(s)\,\mathrm{d}s}{\oint_C K_I^2(s)\,\mathrm{d}s}} = K_{Ic} \tag{8}$$

2.2. *Elliptical crack: iso-stress crack growth by SIF values*

As a particular case, we consider the elliptical flat crack shown in Figure 3a. The failure stress according to LEFM assuming an iso-stress crack growth is here obtained by the results in Section 2.1 (Equation (8)). The ellipse in Figure 3b is defined by semi-axes a and b ($a \geq b$) defined as:

$$\frac{x^2}{a^2} + \frac{y^2}{b^2} = 1 \tag{9}$$

or in parametric form ($0 \leq \varphi < 2\pi$):

$$\mathbf{P}(\varphi) = \begin{cases} x = a\cos\varphi \\ y = b\sin\varphi \end{cases} \tag{10}$$

The aspect of the ellipse is univocally defined either by the aspect ratio $\gamma = b/a$ ($0 < \gamma < 1$) or by the eccentricity $k = \sqrt{1-(b/a)^2}$ ($0 < k < 1$).

The SIF along the crack front is [32]:

$$K_I = \frac{\sigma\sqrt{\pi b}}{E(k^2)}\sqrt[4]{1-k^2\cos^2\varphi} \tag{11}$$

where $E(k_2)$ is the complete elliptic integral of the second kind (see Appendix B). From Equation (11) the maximum value of the SIF $K_{I,\max}$ is at point B (i.e. on the minor axis, $\varphi = \pi/2$) while the minimum value of the SIF $K_{I,\min}$ is at point A (i.e. on the major axis, $\varphi = 0$):

$$K_{I,\max} = (K_I)_B = \frac{\sigma\sqrt{\pi b}}{E(k^2)} \tag{12}$$

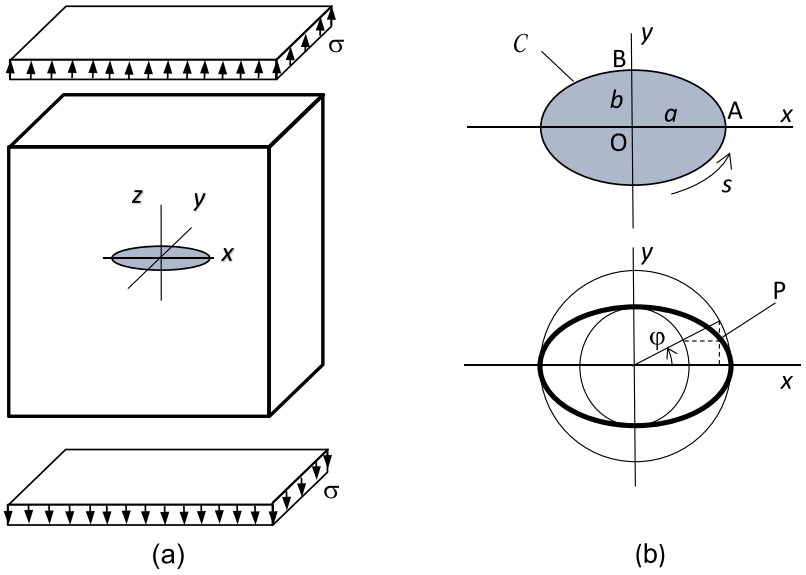

Figure 3. An elliptical (planar) crack in an infinite medium under uniform tensile stress normal to the crack plane (a). Crack geometry (b).

$$K_{I,\min} = (K_I)_{\mathrm{A}} = \frac{\sigma b}{E(k^2)}\sqrt{\frac{\pi}{a}} = K_{I,\max}\sqrt{\frac{b}{a}} \tag{13}$$

For what concerns $K_{I,\max}$, Equation (12) encompasses the limit cases of a penny-shaped crack ($k = 0$ or $\gamma = 1$):

$$K_I = \frac{2}{\pi}\sigma\sqrt{\pi b} \tag{14}$$

constant all around the crack front, and of a through-the-thickness crack of length $2b$ (corresponding to $k = 1$ or $\gamma = 0$):

$$K_I = \sigma\sqrt{\pi b} \tag{15}$$

To obtain the failure stress, we have to compute the 2D-equivalent SIF by means of Equation (8). Using the parametric expression of the ellipse (Equation (10)), the equivalent SIF (Equation (8)) reads:

$$K_{I,\mathrm{iso}} = \sqrt{\frac{\int_0^{\pi/2} K_I^4(\varphi)\left\|\frac{\mathrm{d}\mathbf{P}}{\mathrm{d}\varphi}\right\|\mathrm{d}\varphi}{\int_0^{\pi/2} K_I^2(\varphi)\left\|\frac{\mathrm{d}\mathbf{P}}{\mathrm{d}\varphi}\right\|\mathrm{d}\varphi}} = \frac{\sigma\sqrt{\pi b}}{E(k^2)}\sqrt{\frac{\int_0^{\pi/2}\left(1-k^2\cos^2\varphi\right)^{3/2}\mathrm{d}\varphi}{\int_0^{\pi/2}\left(1-k^2\cos^2\varphi\right)\mathrm{d}\varphi}} \tag{16}$$

where the double symmetry of the ellipse has been exploited to limit the integration interval to $[0,\pi/2]$. By analytical manipulations, the integrals in Equation (16) can be cast in terms of complete elliptic integrals of first ($K(k^2)$) and second ($E(k^2)$) kind (see Appendix B) as:

$$K_{I,\mathrm{iso}} = \frac{2\sigma\sqrt{b}}{E(k^2)}\sqrt{\frac{2(2-k^2)E(k^2)-(1-k^2)K(k^2)}{3(2-k^2)}} \tag{17}$$

Thus, according to LEFM and iso-stress crack growth, failure is achieved whenever the above quantity reaches the material fracture toughness. Hence, the corresponding failure stress $(\sigma_{\mathrm{f}})_{\text{LEFM-iso}}$ is:

$$(\sigma_{\mathrm{f}})_{\text{LEFM-iso}} = \frac{\sqrt{3}}{2}\frac{K_{\mathrm{Ic}}}{\sqrt{b}}E(k^2)\sqrt{\frac{2-k^2}{2(2-k^2)E(k^2)-(1-k^2)K(k^2)}} \tag{18}$$

Note that, as expected for any LEFM approach, the failure stress tends to infinity as the crack vanishes (i.e. $\sigma_f \to \infty$ as $b \to 0$).

2.3. *Elliptical crack: iso-stress crack growth by SERR evaluation*

We show in this sub-section that same results in Section 2.2 are obtained also by proper evaluation of the SERR. This procedure will be exploited in the following to remove the assumption of iso-stress crack growth.

Computation of the SERR G can be performed without the need of SIF (i.e. without exploiting Irwin's relationship). It is the way followed originally by Griffith in his 1921 seminal work. Accordingly, under load control, one has:

$$G = \lim_{\Delta A \to 0} \frac{\Delta \Phi}{\Delta A} \tag{19}$$

To compute G_{iso} (i.e. the SERR assuming an iso-stress crack growth) by Equation (19) one need to know (i) the iso-stress contour lines and (ii) the change in strain energy $\Delta\Phi$ due to the (finite) variation ΔA of the crack surface. These ingredients can be derived by Green and Sneddon [30] solution. Accordingly, because of the remote stress the planar elliptical crack takes the shape of an ellipsoid whose semi-axes are a, b and $w_{\max}$ (the maximum crack opening displacement), the last one given by:

$$w_{\max} = \frac{2\sigma b}{E(k^2)E'} \tag{20}$$

By looking at the load as a uniform remote tensile stress field plus a uniform compressive stress applied on the crack faces, and by means of Clapeyron's theorem, the strain energy Φ increment due to the presence of the crack can be computed as:

$$\Phi = \frac{\sigma V}{2} \tag{21}$$

where V is the volume of the (deformed) crack (i.e. the ellipsoid), whose value is:

$$V = \tfrac{4}{3}\pi a\, b\, w_{\max} \tag{22}$$

Hence, by combining Equations (20) to (22):

$$\Phi = \frac{4\pi}{3E(k^2)} \frac{\sigma^2 a b^2}{E'} \tag{23}$$

The iso-stress lines can also be derived from Green and Sneddon [30]. From their solution, the σ_z stress field on the crack plane (outside the crack faces) is amenable of the following analytical expression:

$$\frac{\sigma_z}{\sigma} = 1 + \frac{1}{E(k^2)} \left[\frac{a}{\sqrt{\xi}} \sqrt{\frac{b^2+\xi}{a^2+\xi}} - E\left(\arcsin \frac{a}{\sqrt{a^2+\xi}} | \, k^2 \right) \right] \tag{24}$$

where $E(\varphi|k^2)$ is the incomplete elliptic integral of the second kind (see Appendix B) and ξ is an ellipsoidal coordinate. On the crack plane ($z = 0$), ξ = constant ($\xi \geq 0$) corresponds to a family of ellipses with equation:

$$\frac{x^2}{a^2+\xi} + \frac{y^2}{b^2+\xi} = 1 \tag{25}$$

Hence, we get a relevant information: *the iso-stress curves are a particular family of ellipses*. More precisely, Equations (24) and (25) show that, as ξ increases from 0 to ∞, the stress value decreases from ∞ to σ and the corresponding isostress lines are ellipses of increasing size and decreasing eccentricity. As an example, some of them are plotted in Figure 4a for an elliptical crack with aspect ratio $\gamma = 0.5$. Naming by Δa and Δb the increment of the semi-axes of the generic iso-stress

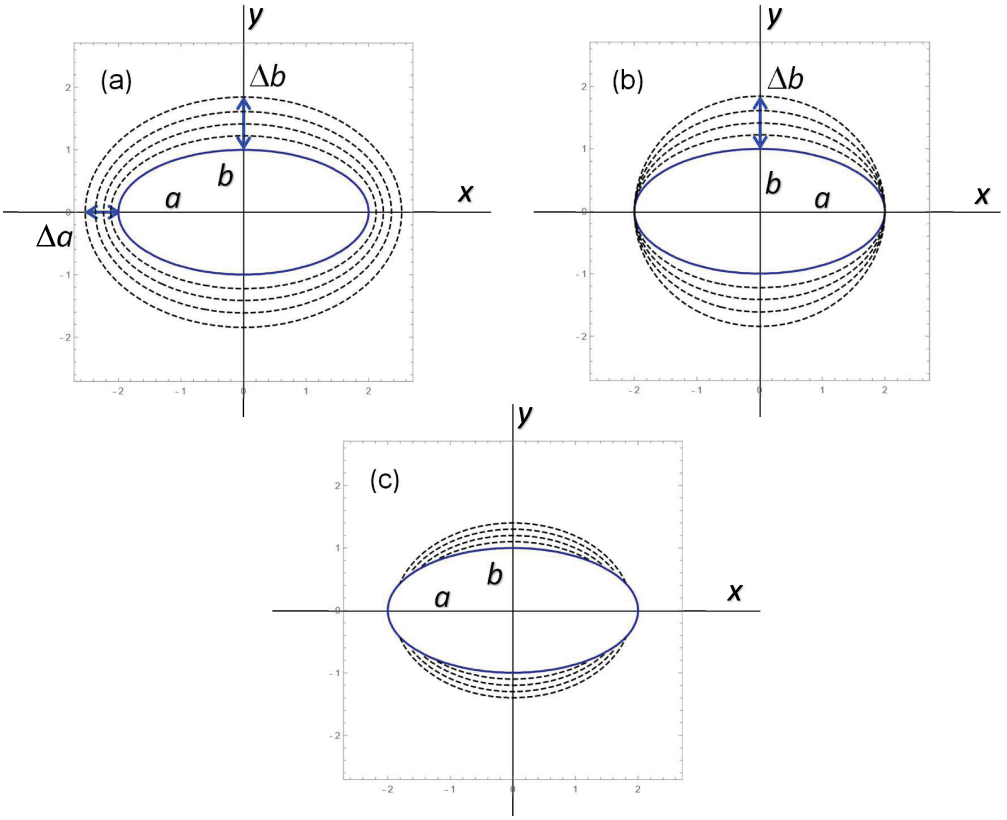

Figure 4. Possible crack growths: (elliptical) *iso-stress crack growth* (a); elliptical, with increment along minor axis alone (b), named *minor-axis crack growth*; non-elliptical crack growth, not considered in the current investigation (c).

line with respect to the ones of the original elliptical flaw, from Equation (25) the relationship between them may be obtained (see details in Appendix C):

$$\Delta a = \sqrt{a^2 + 2b\Delta b + (\Delta b)^2} - a \tag{26}$$

Let us assume the crack grows by a finite amount up to a given iso-stress line, which in turns is defined by a given ξ value. From Equation (23), the energy variation $\Delta\Phi$ is:

$$\Delta\Phi = \frac{4\pi\sigma^2}{3E'}\left\{\frac{\left(b^2+\xi\right)\sqrt{a^2+\xi}}{E\left[(a^2-b^2)/(a^2+\xi)\right]} - \frac{ab^2}{E(1-b^2/a^2)}\right\} \tag{27}$$

while the newly created crack surface is (difference between elliptical areas):

$$\Delta A = \pi\left[\sqrt{a^2+\xi}\sqrt{b^2+\xi} - ab\right] \tag{28}$$

The following step is inserting Equations (27) and (28) into Equation (19). Then, the limit for $\Delta A \to 0$ (i.e. $\xi \to 0$) has to be evaluated. The limit takes the undetermined form 0/0, but the application of De l'Hôpital rule along with property (B4) allows the computation of the limit. Finally equating the SERR G_{iso} to the fracture energy G_{c} along with Irwin relationship yields failure stress $(\sigma_{\text{f}})_{\text{LEFM-iso}}$, which coincides with Equation (18). Thus, despite the different lines of thought (local vs. global), we checked that the SIF- and SERR-based procedures yield the same outcome, Equation (18).

2.4. *Elliptical crack: minor axis crack growth*

On the basis of the analysis in the previous section, we are able to evaluate the failure stress for any elliptical crack growth (i.e. not only the iso-stress crack growth). The criterion that mostly agrees with LEFM is the G-max, i.e. the crack growth actually occurring is the one providing the maximum SERR and consequently the minimum failure stress. Since the SIF is higher at the edge of the minor axis, among all elliptical crack extensions, the one resulting in the largest SERR is the one at which only the minor axis is increasing.

Let us denote by Δb the increment of the minor axis (see Figure 4b). The energy available for a finite elliptical crack growth along the minor axis by Δb is:

$$\Delta\Phi = \frac{4\pi\sigma^2}{3E'}\left\{\frac{a\,(b+\Delta b)^2}{E\left[1-(b+\Delta b)^2/a^2\right]}-\frac{ab^2}{E\left(1-b^2/a^2\right)}\right\} \tag{29}$$

The energy needed to create the new surface is:

$$\Delta\Phi = G_c\pi\left[a\,(b+\Delta b)-ab\right] \tag{30}$$

The corresponding failure stress $(\sigma_f)_{\text{LEFM-minor}}$ is obtained by equating Equations (29)–(30) and taking the limit for $\Delta b \to 0$, or, by introducing the ratio ε_b between the final value of the minor axis and its initial value, letting $\varepsilon_b \to 1$:

$$\varepsilon_b = \frac{b+\Delta b}{b} \tag{31}$$

$$\begin{aligned}(\sigma_f)_{\text{LEFM-minor}} &= \lim_{\varepsilon_b\to 1}\sqrt{\frac{3}{4}\frac{K_{Ic}^2}{b}\frac{\varepsilon_b-1}{\frac{\varepsilon_b^2}{E\left[1-\varepsilon_b^2(1-k^2)\right]}-\frac{1}{E(k^2)}}}\\ &= \frac{\sqrt{3}}{2}\frac{K_{Ic}}{\sqrt{b}}E(k^2)\frac{k}{\sqrt{(1+k^2)E(k^2)-(1-k^2)K(k^2)}}\end{aligned} \tag{32}$$

where again De l'Hôpital rule along with property (B4) has been used.

A further, third, estimate of the failure stress is obtained by setting $K_{I,\max} = K_{Ic}$. This condition is sometime referred to as Irwin criterion (as opposed to the previous ones, based on Equation (19), referred to as Griffith criterion, see e.g. [42]). Note that, differently from 2D problems where the two criteria coincide, the equality $K_{I,\max} = K_{Ic}$ does not rely on any energy balance; however, it is interesting because it provides conservative predictions with respect to the previous estimates Equations (18) and (32). Let us denote $(\sigma_f)_{\text{Irwin}}$ the new failure stress estimate. By Equation (12) one easily obtains:

$$(\sigma_f)_{\text{Irwin}} = K_{Ic}\frac{E(k^2)}{\sqrt{\pi b}} \tag{33}$$

In Figure 5 the dimensionless failure stress estimates Equations (18), (32), (33) are plotted vs. the ellipse eccentricity. Note that all predictions are close, since the contra-harmonic mean (of $G \sim K_I^2$), as already observed, is close to its maximum value. In Figure 5a the estimates are compared at constant minor axis length. As k increases, so does the major axis and, obviously, the failure stress decreases. LEFM based on minor-axis crack growth provides predictions closer (or equal) to G-max criterion: however, we cannot state Equation (32) coincides with G-max criterion since infinitesimal crack extensions other than the elliptical ones could take place (see e.g. Figure 4c). It is apparent that, according to G-max criterion the effective failure stress lies in between Equations (32) (upper bound) and (33) (lower bound). Reasonably, it will be closer to minor-axis crack growth for small eccentricity and closer to Irwin estimate for large eccentricity, where an elliptical crack growth is unlikely: e.g., for $k = 1$, we know the failure stress

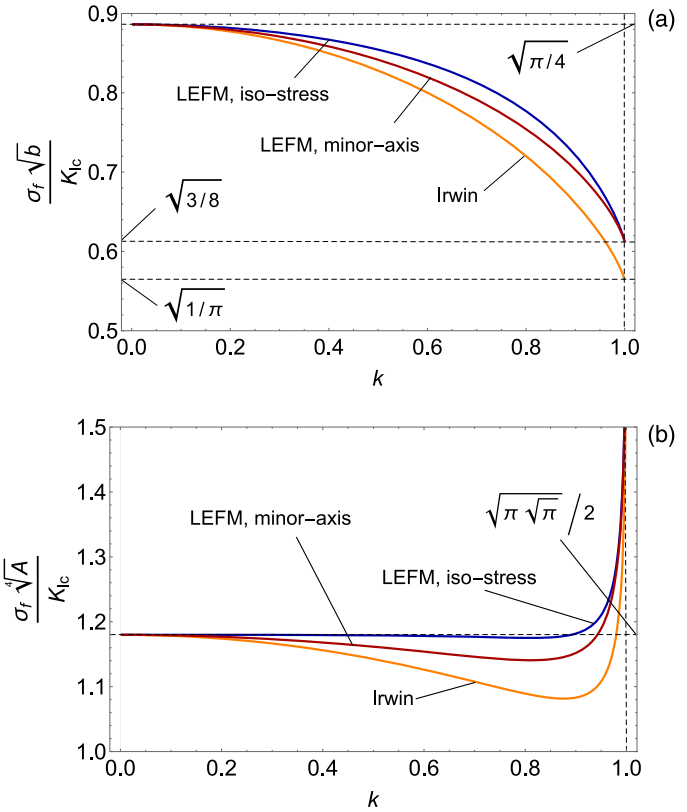

Figure 5. LEFM failure stress estimates vs. ellipse eccentricity k for an infinitesimal iso-stress crack growth (LEFM, iso-stress), an infinitesimal minor axis crack growth (LEFM, minor-axis), $K_{I,\max} = K_{Ic}$ (Irwin): at constant defect minor axis b (a) and at constant defect area A (b); $k = 0$ refers to a penny-shaped crack while $k = 1$ refers to a through-the-thickness crack.

is $\sigma_f = K_{Ic}/\sqrt{(\pi b)}$, since the geometry becomes the 2b-long through-the-thickness crack, while LEFM-minor (and LEFM-iso) provides $\sigma_f = K_{Ic}\sqrt{3}/\sqrt{(8b)}$, see Figure 5a.

In Figure 5b the same estimates are plotted at constant defect area $A = \pi ab$. It is evident that the effect of eccentricity is very low up to eccentricity values close to unity, i.e. what really affect failure stress is the defect area and not its shape. This result agrees with the ones provided by David and Lazarus [43], related to (flat) defects of almost any shape.

3. FFM approach

The estimates provided in the previous section are based on a LEFM approach. As such, they share the well-known drawback that can be applied only to cracked bodies, or, the same, they provide infinite failure stress as the defect size vanishes. On the other hand, for quasi-brittle materials, we expect the failure stress to approach the material tensile strength σ_c as the defect size vanishes. Thus, more refined models able to take into account the material tensile strength beyond the fracture toughness (or fracture energy) have to be used to deal with defects of any size. Herein, we resort to the CCFFM, whose predictions will match LEFM just for relatively large defect size, where energy alone rules crack growth and propagation.

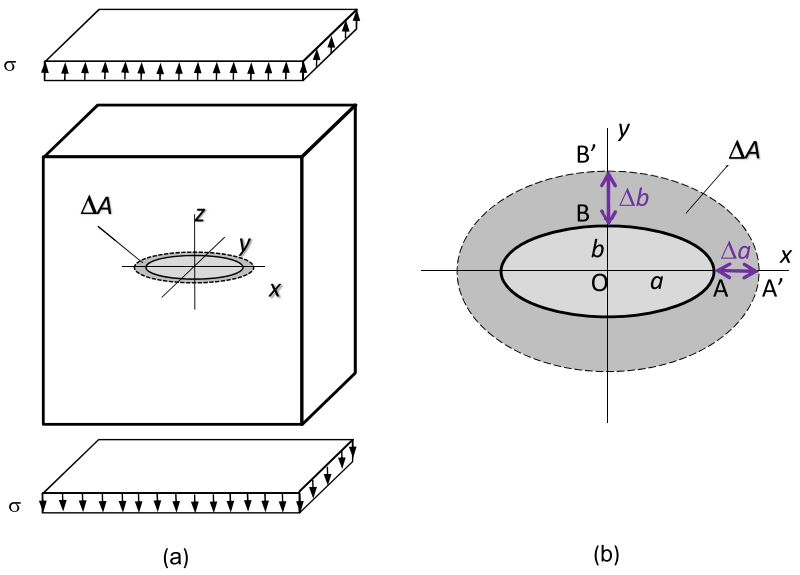

Figure 6. An elliptical (planar) crack in an infinite medium under uniform tensile stress normal to the crack plane: solution by FFM (a); crack geometry and elliptical finite crack growth of any shape (b).

The CCFFM assumes crack growth by a finite increment ΔA (whence the name FFM), see Figure 6a. This increment as well as the failure load are determined based on the finite energy balance and a stress condition (whence the name CC)—the stress must exceed the material tensile strength over the newly created crack surface ΔA. While in 2D the finite crack extension is simply determined by its length and, possibly, by its direction, in 3D problems the crack extension can have any shape (the actual one will be the one minimising the failure load), even in cases where the crack plane is already known, as in the present case. The application of FFM to 3D problems is thus a challenging task. Up to now, a common approach in the literature has been to consider finite crack growth following the iso-stress lines [25,27–29]. This assumption greatly simplifies the problem, allowing the crack growth to be described by just one parameter; moreover, it makes the fulfilment of the stress requirement trivially checked. However, a check of the approximation introduced by considering just (finite) iso-stress crack growths is not available; our goal is to provide it for the model problem at hand (the flat elliptical crack).

Thus, let us derive the CCFFM failure stress for the planar elliptical crack (Figure 2). Here we don't restrict the analysis to finite iso-stress crack growth, since the results in the previous section allow us to consider the crack growth of any (yet elliptical) shape.

Hence, let us assume a finite crack growth where the new crack front has the shape of an ellipse (see Figure 6b) (whose symmetry axes coincide with the ones of the original flaw elliptical geometry). Its shape is univocally determined by two parameters, namely the increment of the minor axis Δb and the increment of the major axis Δa. As such, this approach includes as particular cases the iso-stress crack growth (Figure 4a) and the minor-axis crack growth (Figure 4b). Since the iso-stress lines are also elliptical, the lowest stress level within the crack extension (darker area in Figure 6) is reached either at A' or B' (Figure 6b). Thus, in order the stress condition to be fulfilled, it is enough to check that $\sigma_z(A') \geq \sigma_c$ and $\sigma_z(B') \geq \sigma_c$; meanwhile FFM also requires that the energy available for crack growth $\Delta\Phi$ is larger than the

energy dissipated to create the new fracture surface ΔA. That is:

$$\begin{cases} \sigma_z(A') \geq \sigma_c \\ \sigma_z(B') \geq \sigma_c \\ \Delta\Phi \geq G_c \Delta A \end{cases} \tag{34}$$

It is worth noting the analogy with the approach presented in [44], where the growth of an embedded elliptical crack under fatigue loading was analysed by analytically coupling and solving the Paris laws at points A and B, while assuming that the crack front maintains an elliptical shape throughout its propagation.

Beyond the ratio ε_b between the final value of the minor axis and its initial value—Equation (31)—we now also introduce the ratio ε_a between the final value of the major axis and its initial value:

$$\varepsilon_a = \frac{a + \Delta a}{a} \tag{35}$$

The first inequality in Equation (34) is achieved by means of Equation (24) along with the following ξ value (coming from Equation (25)):

$$\sqrt{a^2 + \xi} = a + \Delta a \Rightarrow \xi = (\varepsilon_a^2 - 1) a^2 \tag{36}$$

yielding (by Equation (35) as well):

$$\frac{\sigma}{\sigma_c} \geq E(k^2) \left[\frac{1}{\varepsilon_a} \sqrt{\frac{\varepsilon_a^2 - k^2}{\varepsilon_a^2 - 1}} + E(k^2) - E\left(\arcsin \frac{1}{\varepsilon_a} \,|\, k^2 \right) \right]^{-1} = f_{Sa}(\varepsilon_a, k^2) \tag{37}$$

The second inequality in Equation (34) is achieved by means of Equation (24) along with the following ξ value (coming again from Equation (25)):

$$\sqrt{b^2 + \xi} = b + \Delta b \Rightarrow \xi = \left(\varepsilon_b^2 - 1\right) b^2 \tag{38}$$

yielding (by Equation (31) as well):

$$\frac{\sigma}{\sigma_c} \geq E(k^2) \left[\frac{\varepsilon_b^2}{\sqrt{\varepsilon_b^2 - 1} \sqrt{\left(1 - k^2\right) \varepsilon_b^2 + k^2}} + E(k^2) - E\left(\arcsin \frac{1}{\sqrt{\left(1 - k^2\right) \varepsilon_b^2 + k^2}} \,|\, k^2 \right) \right]^{-1} = f_{Sb}\left(\varepsilon_b, k^2\right) \tag{39}$$

The third inequality in Equation (34) follows from Equation (23) and the area of the crack increment ΔA:

$$\Delta\Phi = \frac{4\pi}{3} \frac{\sigma^2}{E'} \left\{ \frac{(a + \Delta a)(b + \Delta b)^2}{E\left[1 - \left(\frac{b + \Delta b}{a + \Delta a}\right)^2\right]} - \frac{a b^2}{E\left[1 - \left(\frac{b}{a}\right)^2\right]} \right\} \tag{40}$$

$$\Delta A = \pi \left[(a + \Delta a)(b + \Delta b) - a b \right] \tag{41}$$

Let us introduce the dimensionless flaw size β as:

$$\beta = \frac{b}{(K_{Ic}/\sigma_c)^2} = \frac{b}{l_{ch}} \tag{42}$$

where l_{ch} is (Irwin's) material characteristic length. Equation (42) highlights that the crack size is a relative concept: what really matters is the ratio of the size to the characteristic length. Note also that β is the square of the inverse of the so-called brittleness number introduced by

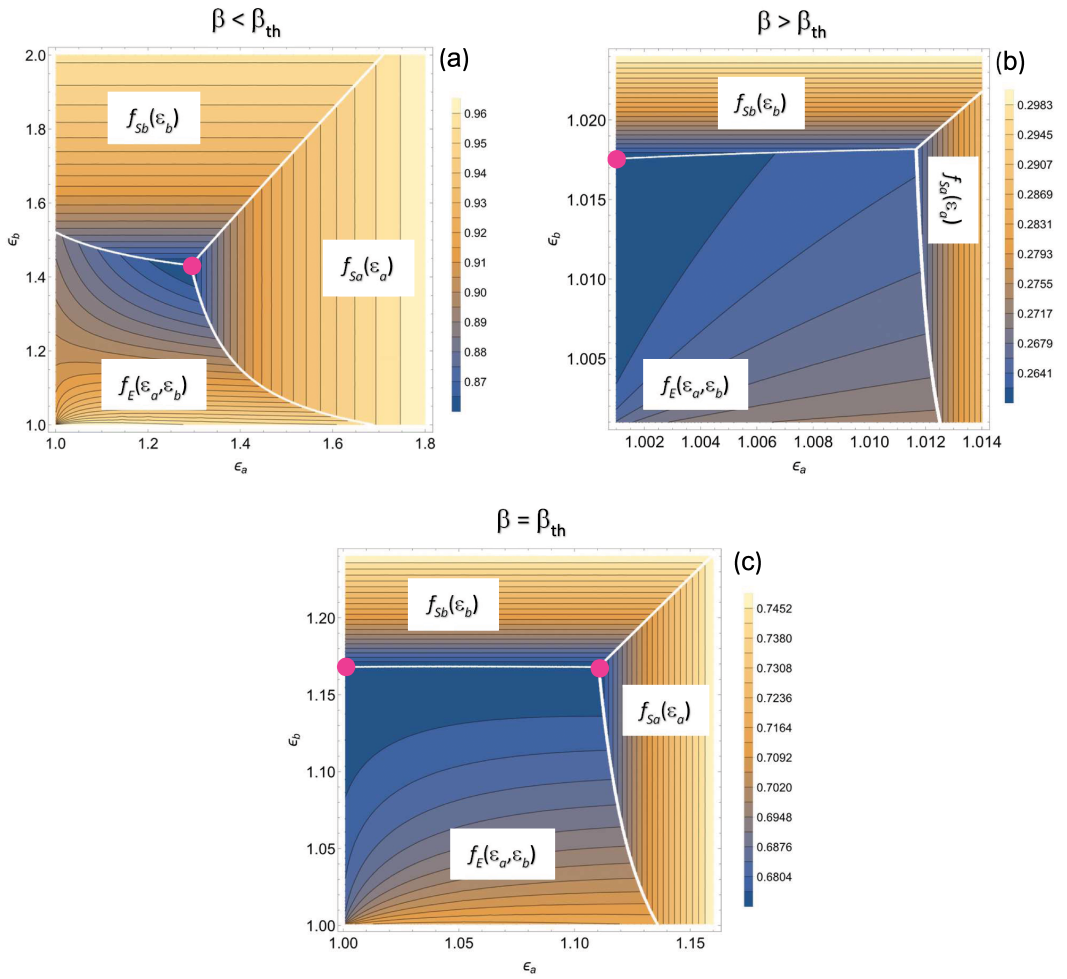

Figure 7. Graphical representation of the minimum search—Equation (44)—for ellipse eccentricity k (flaw shape) equal to 0.8. The dots correspond to the position of the minimum. Small flaw size ($\beta = 0.8$), corresponding to iso-stress crack growth scenario (a); large flaw size ($\beta = 10$), corresponding to minor-axis crack growth scenario (b); limit ($\beta \cong 1.45$) case (c).

Carpinteri [45], $s = K_{\mathrm{Ic}}/(\sigma_{\mathrm{c}}\sqrt{b})$. By Equations (40) and (41), the third inequality in Equation (34) in dimensionless form finally reads:

$$\frac{\sigma}{\sigma_{\mathrm{c}}} \geq \frac{\sqrt{3}}{2\sqrt{\beta}} \sqrt{\frac{\varepsilon_a \varepsilon_b - 1}{\frac{\varepsilon_a \varepsilon_b^2}{E\left[1-\frac{(1-k^2)\varepsilon_b^2}{\varepsilon_a^2}\right]} - \frac{1}{E(k^2)}}} = \frac{1}{\sqrt{\beta}} f_E(\varepsilon_a, \varepsilon_b, k^2) \tag{43}$$

Hence, according to FFM, for a given defect shape (k) and size (β), the relative failure stress $\sigma_{\mathrm{f}}/\sigma_{\mathrm{c}}$ is univocally determined. More precisely, σ_{f} is the minimum value, for any crack increment $\varepsilon_a > 1$ and $\varepsilon_b > 1$, satisfying the three inequalities in Equation (34). That is:

$$\sigma_{\mathrm{f}} = \sigma_{\mathrm{c}} \times \min_{\substack{\varepsilon_a > 1 \\ \varepsilon_b > 1}} \max \left\{ f_{Sa}\left(\varepsilon_a, k^2\right), f_{Sb}\left(\varepsilon_b, k^2\right), \frac{1}{\sqrt{\beta}} f_E\left(\varepsilon_a, \varepsilon_b, k^2\right) \right\} \tag{44}$$

Let us fix k, e.g. $k = 0.8$. Depending on β, we may have just two scenarios, as evident in Figure 7. For small β (Figure 7a), i.e. for relatively small flaw size, the minimum load is achieved for iso-stress crack growth (Figure 4a). The finite crack growth is significant (i.e. ε_a and ε_b significantly larger than unity) and the relationship between the increment of the two semi-axes is given by Equation (26) that, in terms of ε_a and ε_b, can be more conveniently expressed as (see Appendix C for details):

$$\varepsilon_a = \sqrt{k^2 + \left(1 - k^2\right)\varepsilon_b^2} \tag{45}$$

Note that in this case the three inequalities in Equation (34) are strictly fulfilled. This former scenario is the iso-stress one.

The second scenario (Figure 7b) is linked to large β, i.e. for relatively large flaw size: the minimum load is achieved for minor-axis crack growth (Figure 4b). The finite crack growth is relatively small (i.e. ε_b slightly higher than unity) and, of course, $\varepsilon_a = 1$ since there is no increment in the major axis of the flaw. Note that in this latter case the second and third inequalities in Equation (34) are strictly fulfilled while the first one is over fulfilled. This latter scenario is the minor-axis one. The discriminant between the two scenarios is when the failure stress is the same (see Figure 7c), i.e.:

$$f_E\left(\varepsilon_a = 1, \varepsilon_b\right) = f_E\left(\varepsilon_a = \sqrt{k^2 + (1 - k^2)\varepsilon_b^2}, \varepsilon_b\right) \tag{46}$$

This is an equation in the unknown ε_b. Let us name $\overline{\varepsilon}_b$ its solution. The corresponding dimensionless threshold size β_{th} is obtained by equating the stress condition (either the first or the second one in Equation (34)) with the energy one (third condition in Equation (34)). That is:

$$\beta_{\text{th}} = \left[\frac{f_E\left(\varepsilon_a = 1, \overline{\varepsilon}_b\right)}{f_{Sb}\left(\overline{\varepsilon}_b\right)}\right]^2 \tag{47}$$

For $k = 0.8$, we found $\beta_{\text{th}} \cong 1.45$. Then, if $\beta < \beta_{\text{th}}$, iso-stress scenario takes place. Accordingly, the finite crack growth (through ε_b) is given by the solution of the following equation:

$$\sqrt{\beta}\, f_{Sb}\left(\varepsilon_b\right) = f_E\left(\varepsilon_a = \sqrt{k^2 + (1 - k^2)\varepsilon_b^2}, \varepsilon_b\right) \tag{48}$$

On the other hand, if $\beta > \beta_{\text{th}}$, minor-axis scenario takes place. Accordingly, the finite crack growth (through ε_b) is provided by solving:

$$\sqrt{\beta}\, f_{Sb}\left(\varepsilon_b\right) = f_E\left(\varepsilon_a = 1, \varepsilon_b\right) \tag{49}$$

Let us denote by $\varepsilon_{b\text{c}}$ the solution of either Equation (48) or (49). In both cases the failure stress is given by either the stress or energy condition. Taking the first we have:

$$\sigma_{\text{f}} = \sigma_{\text{c}}\, f_{Sb}\left(\varepsilon_{b\text{c}}\right) \tag{50}$$

For clarity, the flow chart providing the finite crack growth and the failure stress is given in Figure 8.

In Figure 9 the failure stress vs. flaw size plots for different ellipse eccentricity values are drawn. The threshold size according to which there is the switch between scenarios is also highlighted. While the iso-stress scenario prevails for small eccentricity (being the only one for a penny-shaped crack), the minor-axis scenario becomes predominant for large eccentricity. Note also that FFM reverts to LEFM (in its minor-axis crack growth version) as the flaw size increases; on the other hand, for small flaw size, LEFM provides unrealistically high failure stresses, while FFM predictions remain always lower than the material tensile strength.

In Figure 10a the different curves in Figure 9 are compared altogether, including the ones referring to a through-the-thickness crack of semi-length b ($k = 1$) and to a penny-shaped crack of radius b ($k = 0$). Note that these two latter cases are 2D geometries (the first one is actually a 2D problem; the second one is a pseudo 3D problem, due to the radial symmetry); as such,

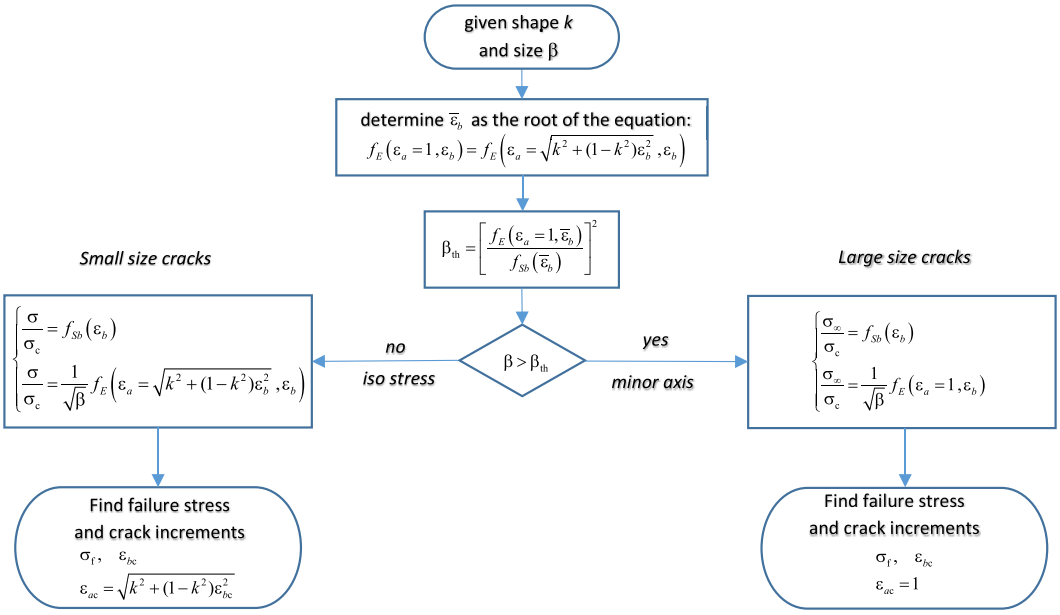

Figure 8. Flowchart to determine the failure stress σ_f for a given flaw shape (k) and size (β).

their solution is simpler and already available in the literature [16,17]. Of course, the comparison being made at constant b, the failure stress decreases as the eccentricity increases. In Figure 10b the same comparison is provided at a constant flaw area (the through-the-thickness crack case is somewhat meaningless, since A constant and a infinite yield b null). Again, as in the LEFM analysis, it is apparent that, for relatively small eccentricity, the parameter governing failure stress is the flaw area. In other words, for flaw aspect ratio b/a between 0.5 and 1, the failure stress due to the presence of an elliptical crack is (almost) equal to the one due to a penny-shaped crack of the same area.

Note that, whatever is the scenario, the elliptical crack always grows toward an elliptical shape closer to that of a circle (with respect to the original elliptical shape), i.e. the eccentricity diminishes. This is a common finding in the literature, even for original flaws of shape other than the elliptical one [35,38,43,44].

Regarding the difference between iso-stress and non-iso-stress finite crack growth, for small sizes fracture propagates actually by iso-stress lines. For larger size (i.e. $\beta > \beta_{th}$) the iso-stress failure stress prediction becomes larger than the minor axis one. Let us consider for instance the case considered in Figure 7b, where $k = 0.8$ and $\beta = 10$: although it is clear that the minimum load is achieved for minor-axis growth ($\varepsilon_a = 1$), it is also apparent that the failure stress corresponding to iso-stress crack growth is just slightly larger. Actually the difference between the two predictions increases with size, i.e. β. For $\beta \to \infty$, FFM reverts to LEFM and the difference between minor-axis and iso-stress predictions can be directly determined from Figure 5a. For instance, for $k = 0.8$, the relative difference (i.e. the error made using the iso-stress assumption) is about 3%, which is almost negligible from an engineering point of view. Figure 5a also shows that the largest error takes place when $\beta \to \infty$ and $k = 1$, i.e. a large through-the-thickness crack: in this extreme case the difference is $[\sqrt{(3/8)} - \sqrt{(1/\pi)}/\sqrt{(1/\pi)}] \cong 8.5\%$. Thus, we can conclude that, for the geometry at hand and for ellipse aspect ratios not really close to zero (i.e. except for case $b \ll a$), the error made by using the iso-stress crack growth assumption is reasonably small. Of course, this does not mean that this is always the case, but the present case corroborates the

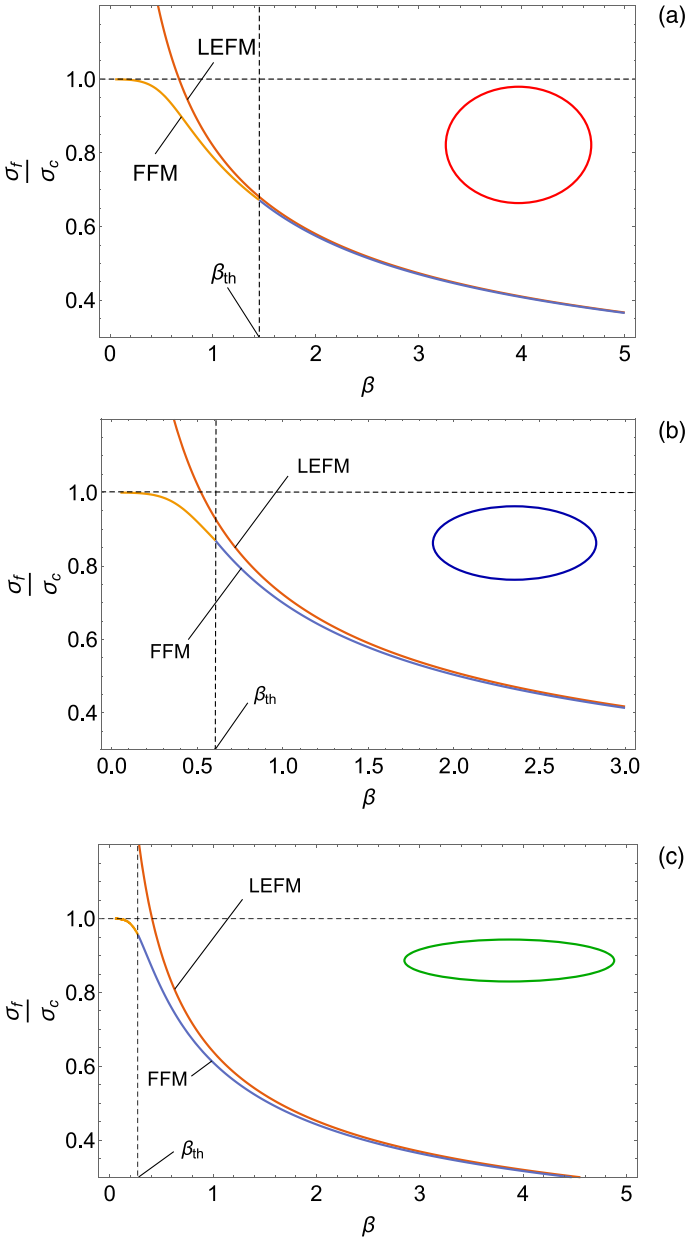

Figure 9. Failure stress vs. dimensionless flaw size $\beta = b/l_{ch}$ for different flaw shape (i.e. ellipse eccentricity k or aspect ratio $\gamma = b/a$) according to LEFM (minor axis crack growth) and to FFM: $\gamma = 0.8$, $k = 0.6$ (a); $\gamma = 0.5$, $k \cong 0.85$ (b); $\gamma = 0.2$, $k \cong 0.98$ (c). Threshold value of β dividing iso-stress (left) and minor axis (right) finite crack growth are also highlighted.

conjecture made by Leguillon [25], i.e. iso-stress crack growth can be a reasonable and effective simplifying assumption.

Finally, note that extending our analysis to a more complex stress state, such as the one occurring to the present geometry when the remote tensile stress is not normal to the crack plane, would broaden the applicability of the paper. However, given the mode mixity (I, II, III)

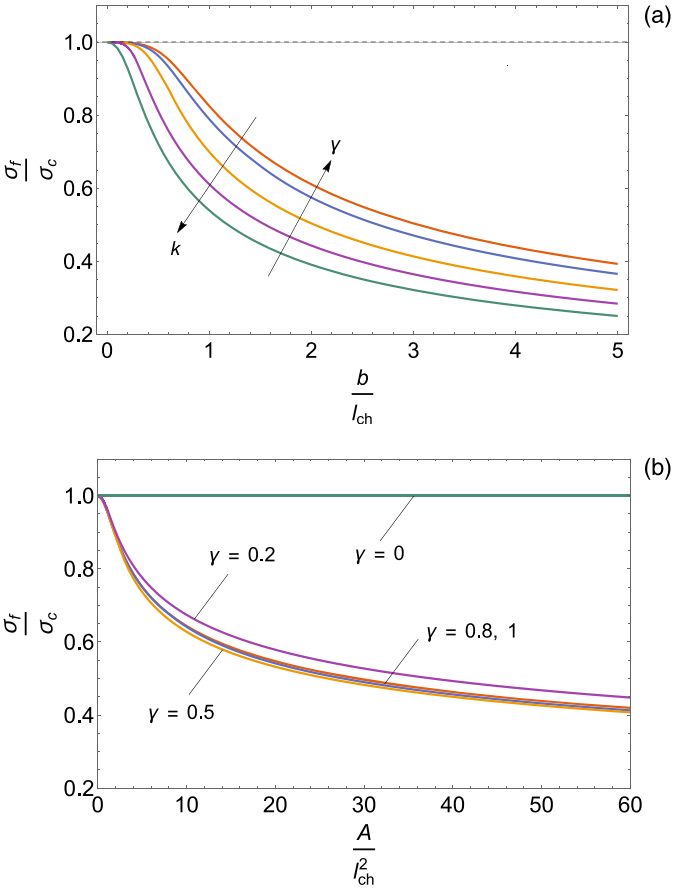

Figure 10. FFM estimates of the failure stress for different flaw shape ($k \cong 0$, 0.6, 0.85, 0.98, 1; i.e. $\gamma = 1$, 0.8, 0.5, 0.2, 0) vs. dimensionless flaw size $\beta = b/l_{ch}$ (a) and vs. dimensionless flaw area (A/l_{ch}^2) (b).

and the expected non-planar (unknown) crack growth, this is a major, challenging task going beyond the scope of the current manuscript. In this sense, it would be reasonable to start with an inclined penny shaped crack, which is a configuration investigated in the past with simpler fracture criteria, see e.g. [46]; see also [47] for recent interesting experimental data.

4. Conclusions

The failure remote stress causing (unstable) crack propagation in an infinite linear elastic 3D domain containing a flat elliptical crack has been obtained in an analytical form by means of the CCFFM, under the assumption that the finite crack growth can be of any elliptical shape. It is found that finite crack growth always leads to elliptical crack geometries with lower eccentricity, i.e. the crack shape tends to that of a penny-shaped crack. Differently from other investigations available in the literature, in this 3D application of FFM we removed the assumption of iso-stress crack growth. Particularly for large flaws we found failure stress values lower than the ones obtained by the iso-stress assumption, which, thus, must be seen as potentially dangerous since providing non-conservative predictions. Nevertheless, the difference appears to be of a few percents and, thus, the iso-stress assumption when applying CCFFM is regarded as more

than reasonable in engineering practice. It is noteworthy that for small elliptical defects, the failure remote stress predicted by the present FFM procedure can be significantly smaller than that obtained by LEFM assuming infinitesimal crack growth. Notably, the failure remote stress predicted by LEFM depends on the assumed shape of the infinitesimal crack increment.

Declaration of interests

The authors do not work for, advise, own shares in, or receive funds from any organization that could benefit from this article, and have declared no affiliations other than their research organizations.

Acknowledgements

The present manuscript is the final version of what presented in the Sevilla workshop within NEWFRAC Project (Marie Sklodowska-Curie grant agreement No. 861061), which is gratefully acknowledged by all the Authors, and later, at the International Conference of Fracture held in Atlanta, June 2023 (ICF15). In Atlanta the Authors had—as usual—fruitful and stimulating discussions about the topic investigated in the present manuscript with Prof. Dominique Leguillon: although he passed away, we wish to thank him and dedicate the present work to his memory. ZY is grateful for the partial support of this research by the Pazy Research Foundation. The research of VM was partially supported by the Spanish Ministry of Science and Innovation and the European Regional Development Fund (PID2021-123325OB-I00). Finally, PC wishes to thank also Prof. Veronique Lazarus for pleasant and useful discussions had at Sorbonne Université, where he was upon Prof. Leguillon's invitation.

Appendix A.

The Contra-harmonic mean (C) was introduced by Eudoxus from Cnidus (408–355 B.C.) as the ratio between the sum of the squares of the values and the sum of the values themselves. The name is due to the fact that, if we consider two values a and b, the distance between the Arithmetic mean (A) and the Harmonic mean (H) is equal to the one between the Contra-harmonic mean (C) and the Arithmetic mean (A):

$$A(a,b) = \frac{a+b}{2} \tag{A1}$$

$$H(a,b) = \frac{2}{1/a+1/b} \tag{A2}$$

$$C(a,b) = \frac{a^2+b^2}{a+b} \tag{A3}$$

$$C(a,b) - A(a,b) = A(a,b) - H(a,b) \tag{A4}$$

For instance, if $a = 9$ and $b = 1$, $A = 5$, $H = 1.8$, $C = 8.2$ ($C-A = 3.2 = A-H$).

Appendix B.

The complete elliptic integral of the first kind reads:

$$K(m) = \int_0^{\pi/2} \frac{1}{\sqrt{1-m\sin^2\varphi}}\,\mathrm{d}\varphi \tag{B1}$$

The complete elliptic integral of the second kind reads:

$$E(m) = \int_0^{\pi/2} \sqrt{1 - m\sin^2\varphi}\,\mathrm{d}\varphi \tag{B2}$$

The derivative of the elliptic integral of the second kind with respect to m is:

$$\frac{\mathrm{d}E(m)}{\mathrm{d}m} = \frac{E(m) - K(m)}{2m} \tag{B3}$$

The incomplete elliptic integral of the second kind is:

$$E\left(\varphi \mid m\right) = \int_0^{\varphi} \sqrt{1 - m\sin^2\vartheta}\,\mathrm{d}\vartheta \tag{B4}$$

The relationship between the incomplete elliptic integral and its complete counterpart is:

$$E\left(\frac{\pi}{2} \mid m\right) = E(m) \tag{B5}$$

Appendix C.

Here we derive the relationship between the semi-axes increments in case of iso-stress crack growth, in dimensional—Equation (26)—and dimensionless—Equation (45)—form.

From Equation (36) we have:

$$\Delta a = \sqrt{a^2 + \xi} - a \tag{C1}$$

while, from Equation (38):

$$\xi = (\Delta b + b)^2 - b^2 \tag{C2}$$

Replacing (C2) into (C1), we get Equation (26).

From Equation (36) we have also:

$$\varepsilon_a^2 = \frac{\xi}{a^2} + 1 \tag{C3}$$

while, from Equation (38):

$$\xi = b^2\left(\varepsilon_b^2 - 1\right) \tag{C4}$$

Replacing (C4) into (C3) and recalling that, by eccentricity definition, $(b/a)^2 = 1 - k^2$, we get Equation (45).

References

[1] D. Leguillon, "Strength or toughness? A criterion for crack onset at a notch", *Eur. J. Mech. A/Solids* **21** (2002), pp. 61–72.

[2] P. Cornetti, N. Pugno, A. Carpinteri and D. Taylor, "Finite fracture mechanics: a coupled stress and e nergy failure criterion", *Eng. Fract. Mech.* **73** (2006), pp. 2021–2033.

[3] Z. Yosibash, E. Priel and D. Leguillon, "A failure criterion for brittle elastic materials under mixed-mode loading", *Int. J. Fract.* **141** (2006), pp. 291–312.

[4] P. Cornetti, A. Sapora and A. Carpinteri, "Mode mixity and size effect in V-notched structures", *Int. J. Solids Struct.* **50** (2013), pp. 1562–1582.

[5] P. Lazzarin, A. Campagnolo and F. Berto, "A comparison among some recent energy- and stress-based criteria for the fracture assessment of sharp V-notched components under mode I loading", *Theor. Appl. Fract. Mech.* **71** (2014), pp. 21–30.

[6] V. Mantič, "Interface crack onset at a circular cylindrical inclusion under a remote transverse tension. Application of a coupled stress and energy criterion", *Int. J. Solids Struct.* **46** (2009), pp. 1287–1304.

[7] E. Martin, D. Leguillon and N. Carrère, "A twofold strength and toughness criterion for the onset of free-edge shear delamination in angle-ply laminates", *Int. J. Solids Struct.* **47** (2010), pp. 1297–1305.

[8] P. P. Camanho, G. H. Erçin, G. Catalanotti, S. Mahdi and P. Linde, "A finite fracture mechanics model for the prediction of the open-hole strength of composite laminates", *Compos.-A: Appl. Sci. Manuf.* **43** (2012), pp. 1219–1225.

[9] P. Weissgraeber and W. Becker, "Finite Fracture Mechanics model for mixed mode fracture in adhesive joints", *Int. J. Solids Struct.* **50** (2013), pp. 2383–2394.

[10] A. Doitrand, G. Molnár, D. Leguillon, E. Martin and N. Carrère, "Dynamic crack initiation assessment with the coupled criterion", *Eur. J. Mech. A/Solids* **93** (2022), article no. 104483.
[11] A. Chao Correas, P. Cornetti, M. Corrado and A. Sapora, "Finite fracture mechanics extension to dynamic loading scenarios", *Int. J. Fract.* **239** (2023), pp. 149–165.
[12] A. Sapora, P. Cornetti, A. Campagnolo and G. Meneghetti, "Fatigue limit: crack and notch sensitivity by finite fracture mechanics", *Theor. Appl. Fract. Mech.* **105** (2020), article no. 102407.
[13] A. M. Mirzaei, P. Cornetti and A. Sapora, "A novel finite fracture mechanics approach to assess the lifetime of notched components", *Int. J. Fatigue* **173** (2023), article no. 107659.
[14] C. Henninger, D. Leguillon and E. Martin, "Crack initiation at a V-notch-comparison between a brittle fracture criterion and the Dugdale cohesive model", *C. R. Mèc.* **335** (2007), pp. 388–393.
[15] I. G. García, M. Paggi and V. Mantič, "Fiber-size effects on the onset of fiber-matrix debonding under transverse tension: a comparison between cohesive zone and finite fracture mechanics models", *Eng. Fract. Mech.* **115** (2014), pp. 96–110.
[16] P. Cornetti, A. Sapora and A. Carpinteri, "Short cracks and v-notches: finite fracture mechanics vs cohesive crack model", *Eng. Fract. Mech.* **168** (2016), pp. 2–12.
[17] P. Cornetti and A. Sapora, "Penny-shaped cracks by Finite Fracture Mechanics", *Int. J. Fract.* **219** (2019), pp. 153–159.
[18] F. Ferrian, P. Cornetti, L. Marsavina and A. Sapora, "Finite fracture mechanics and cohesive crack model: size effects through a unified formulation", *Frat. Integrità Strut.* **16** (2022), pp. 496–509.
[19] A. Chao Correas, A. Sapora, J. Reinoso, M. Corrado and P. Cornetti, "Coupled versus energetic nonlocal failure criteria: A case study on the crack onset from circular holes under biaxial loadings", *Eur. J. Mech. A/Solids* **101** (2023), article no. 105037.
[20] J. Reinoso, A. Arteiro, M. Paggi and P. P. Camanho, "Strength prediction of notched thin ply laminates using finite fracture mechanics and the phase field approach", *Compos. Sci. Technol.* **150** (2017), pp. 205–216.
[21] G. Molnár, A. Doitrand, R. Estevez and A. Gravouil, "Toughness or strength? Regularization in phase-field fracture explained by the coupled criterion", *Theor. Appl. Fract. Mech.* **109** (2020), article no. 102736.
[22] A. Doitrand, G. Molnár, R. Estevez and A. Gravouil, "Strength based regularization length in phase field fracture", *Theor. Appl. Fract. Mech.* **124** (2023), article no. 103728.
[23] G. Molnár, A. Doitrand and V. Lazarus, "Phase-field simulation and coupled criterion link echelon cracks to internal length in Antiplane shear", *J. Mech. Phys. Solids* **188** (2024), article no. 105675.
[24] S. Jiménez-Alfaro, D. Leguillon, C. Maurini and J. Reinoso, "A dialogue between finite fracture mechanics and phase field approaches to fracture for predicting crack nucleation at the microscale", *Int. J. Fract.* **249** (2025), article no. 13.
[25] D. Leguillon, "An attempt to extend the 2D coupled criterion for crack nucleation in brittle materials to the 3D case", *Theor. Appl. Fract. Mech.* **74** (2014), pp. 7–17.
[26] Z. Yosibash and B. Mittelman, "A 3-D failure initiation criterion from a sharp V-notch edge in elastic brittle structures", *Eur. J. Mech.-A/Solids* **60** (2016), pp. 70–94.
[27] I. G. García, B. J. Carter, A. R. Ingraffea and V. Mantič, "A numerical study of transverse cracking in cross-ply laminates by 3D finite fracture mechanics", *Compos. B: Eng.* **95** (2016), pp. 475–487.
[28] A. Doitrand and D. Leguillon, "3D application of the coupled criterion to crack initiation prediction in epoxy/aluminum specimens under four point bending", *Int. J. Solids Struct.* **143** (2018), pp. 175–182.
[29] A. Doitrand and D. Leguillon, "Comparison between 2D and 3D applications of the coupled criterion to crack initiation prediction in scarf adhesive joints", *Int. J. Adhes. Adhes.* **85** (2018), pp. 69–76.
[30] A. E. Green and I. N. Sneddon, "The distribution of stress in the neighbourhood of a flat elliptical crack in an elastic solid", *Proc. Camb. Philos. Soc.* **46** (1950), pp. 159–164.
[31] I. N. Sneddon, "The distribution of stress in the neighbourhood of a crack in an elastic solid", *Proc. R. Soc. Lond. A* **187** (1946), pp. 229–260.
[32] G. R. Irwin, "Crack-Extension Force for a Part-Through Crack in a Plate", *ASME J. Appl. Mech.* **29** (1962), pp. 654–661.
[33] X. K. Zhu, G. T. Liu and Y. J. Chao, "Three-dimensional stress and displacement fields near an elliptical crack front", *Int. J. Fract.* **109** (2001), pp. 383–401.
[34] Y. Schapira and Z. Yosibash, "Asymptotic solution of the elasticity equations in the vicinity of an elliptical crack front", *Eng. Fract. Mech.* **223** (2020), article no. 106774.
[35] V. Lazarus, "Brittle fracture and fatigue propagation paths of 3D plane cracks under uniform remote tensile loading", *Int. J. Fract.* **122** (2003), pp. 23–46.
[36] B. K. Hachi, Y. Belkacemi, S. Rechak, M. Haboussi and M. Taghite, "Fatigue growth prediction of elliptical cracks in welded joint structure: Hybrid and energy density approach", *Theor. Appl. Fract. Mech.* **54** (2010), pp. 11–18.

[37] M. Morishita, K. Gotoh, Y. Anai, S. Tsumura and T. Niwa, "Fatigue surface crack growth behavior in flat plate and out-of-plane gusset-welded joints under biaxial cyclic loads with different phases", *J. Mar. Sci. Technol.* **26** (2021), pp. 655–672.

[38] G. Villani, V. G. Belardi, P. Salvini and F. Vivio, "Energetic approach to predict the elliptical crack growth", *Procedia Struct. Integr.* **47** (2023), pp. 873–881.

[39] M. Burhan, T. Scalici, Z. Ullah, Z. Kazancí and G. Catalanotti, "A three-dimensional Finite Fracture Mechanics model to predict free edge delamination in angle-ply laminates", *Eng. Fract. Mech.* **306** (2024), article no. 110156.

[40] M. Burhan, Z. Ullah, Z. Kazancí and G. Catalanotti, "A finite fracture mechanics approach to assess the fatigue life of laminates exhibiting free edge effects", *Compos. Struct.* **354** (2025), article no. 118797.

[41] M. Burhan, Z. Ullah, Z. Kazancí and G. Catalanotti, "Predicting free edge delamination induced by thermal loading using finite fracture mechanics", *Int. J. Fract.* **250** (2025), article no. 110156.

[42] M. Bach, S. Nazarov and W. Wendland, "Stable propagation of a mode-1 planar crack in an isotropic elastic space. Comparison of the Irwin and the Griffith approaches", in *Problemi Attuali Dell'Analisi e Della Fisica Matematica. Atti del 20 Simposio internazionale (Taormina 15–18 Ottobre 1998)* (P. E. Ricci, ed.), Aracne: Rome, 2000, pp. 167–190.

[43] L. David and V. Lazarus, "On the key role of crack surface area on the lifetime of arbitrarily shaped flat cracks", *Int. J. Fatigue* **154** (2022), article no. 106512.

[44] Y. Mikata, "Analytical solution for fatigue crack propagation of an embedded elliptical crack", *Int. J. Fract.* **229** (2021), pp. 245–251.

[45] A. Carpinteri, "Static and energetic fracture parameters for rocks and concrete", *Mater. Struct.* **14** (1981), pp. 151–162.

[46] J. P. Pereira, C. A. Duarte and X. Jiao, "Three-dimensional crack growth with hp-generalized finite element and face offsetting methods", *Comput. Mech.* **46** (2010), pp. 431–453.

[47] J. Xu, H. Li, H. Wang and L. Tang, "Experimental study on 3D internal penny-shaped crack propagation in brittle materials under uniaxial compression", *Deep Undergr. Sci. Eng.* **2** (2023), pp. 37–51.